RADIO SCIENCE, VOL. 43, RS4005, doi:10.1029/2007RS003760, 2008

Correlative study of plasma bubbles, evening equatorial ionization anomaly, and equatorial prereversal E × B drifts at solar maximum

Guozhu Li,[1] Baiqi Ning,[1] Libo Liu,[1] Biqiang Zhao,[1] Xinan Yue,[1] S.-Y. Su,[2] and Sarita Venkatraman[3]

Received 15 October 2007; revised 10 April 2008; accepted 17 April 2008; published 6 August 2008.

[1] Previous ground observations have revealed a correlation that exists between equatorial plasma bubbles, evening equatorial ionization anomaly (EIA), and prereversal **E** × **B** drift velocity using latitudinal arrays of ionospheric sounders, such as in the Indian and American regions. Besides the ground measurements, the space-based observations also provide a convenient way to study the global-scale variations. On the basis of in situ data collected from DMSP, ROCSAT-1, and CHAMP satellites, we investigated the correlation of seasonal/longitudinal variations of plasma bubble (PB) occurrence, evening EIA, and prereversal **E** × **B** drifts on magnetically quiet days during the solar maximum years (2000–2002). In general, the observational results provide consistent evidences that the large-scale variations in seasonal/longitudinal distribution of evening EIA and PB occurrence rates are well-correlated with the observed evening prereversal **E** × **B** drifts and that some of the small-scale longitudinal variations (such as wave number-4 structure during equinox) of evening EIA exist before the occurrence of the prereversal enhancement and coincide with the daytime equatorial electrojet. In such cases, the small-scale longitudinal variation of PB occurrence rates may result from the evening EIA small-scale longitudinal structures. The evening prereversal **E** × **B** drifts, together with the longitudinal variations of evening EIA, are assumed to play a role in determining the longitudinal variations of equatorial and low-latitude PB occurrence rates.

Citation: Li, G., B. Ning, L. Liu, B. Zhao, X. Yue, S.-Y. Su, and S. Venkatraman (2008), Correlative study of plasma bubbles, evening equatorial ionization anomaly, and equatorial prereversal **E** × **B** drifts at solar maximum, *Radio Sci.*, *43*, RS4005, doi:10.1029/2007RS003760.

1. Introduction

[2] The equatorial and low-latitude ionosphere is a highly dynamic region, which is characterized by the existence of the equatorial ionization anomaly (EIA), shown as a peak in the ion densities located on either side of the magnetic equator, and intense equatorial plasma bubbles (EPBs) associated with irregularities inducing ionospheric scintillation. The EIA is known to be created by the fountain effect, which consists of the uplift of plasma at the magnetic equator by eastward electric fields and subsequent redistribution along the magnetic field lines to higher latitudes. The bubble refers to irregular plasma density depletions observed by satellites and radar backscatter in the topside ionosphere [*Woodman and LaHoz*, 1976], which is generated on the bottomside of the nighttime equatorial *F* region and rises to higher altitudes as a result of nonlinear evolution of the generalized Rayleigh-Taylor (RT) and **E** × **B** instabilities [*Kelley*, 1989; *Fejer et al.*, 1999].

[3] There are a few observational studies on equatorial spread F (ESF) and EIA [e.g., *Walker*, 1981; *Valladares et al.*, 2001; *Dabas et al.*, 2006]. Related study of the association between postsunset EIA, ESF/scintillation and **E** × **B** drift velocity is also reported. *Alex et al.* [1989, 2003] investigated the correlation of EIA and scintillation during ATS-6 phase II in India and during

[1]Beijing National Observatory of Space Environment, Institute of Geology and Geophysics, Chinese Academy of Sciences, Beijing, China.
[2]Institute of Space Science, National Central University, Chung-Li, Taiwan.
[3]William B. Hanson Center for Space Sciences, University of Texas at Dallas, Richardson, Texas, USA.

0048-6604/08/2007RS003760$11.00

IGY in America. In a case study, *Whalen* [2000] used multistation ionosonde data from the American sector and examined the evolution of EPB in relation to the bottomside spread F and to the occurrence of postsunset EIA. Their study reported that there is a strong link between altitudinal/latitudinal growth of a plasma bubble and the development of postsunset EIA. By using ETS-II data at Delhi, *Gupta et al.* [2002] reported that the occurrence of VHF scintillations and Faraday polarization fluctuations are strongly dependent on the simultaneous occurrence of postsunset EIA.

[4] Many observations also show the association of the generation and evolution of ESF with the vertical plasma drift velocities. *Basu et al.* [1996], using the campaign measurements between 25 September to 7 October in 1994 in the South American sector, reported that the prereversal enhancement in upward drift of about 20 m/s is a necessary condition for the development of scintillation occurrence. *Fejer et al.* [1999] analyzed the Jicamarca incoherent scatter radar observations between 1968 and 1992, and found that weak and strong irregularity levels increased with increasing $\mathbf{E} \times \mathbf{B}$ drift. By examining the relationship between the enhanced upward $\mathbf{E} \times \mathbf{B}$ drift velocity after sunset and the subsequent scintillation activity for the forecasting on a day-to-day basis, *Anderson et al.* [2004] demonstrated that there exists a threshold velocity of 20 m/s that determines the scintillation occurrence. *Tulasi Ram et al.* [2006] further confirmed the existence of a threshold value of 30 m/s and 20 m/s respectively during high and low sunspot year in the Indian longitude sector. Taking into consideration the relationship between postsunset EIA and $\mathbf{E} \times \mathbf{B}$ drift, *Garg et al.* [1983] reported that the onset and decay of postsunset EIA is controlled by $\mathbf{E} \times \mathbf{B}$ drifts and meridional winds.

[5] By investigating the joint measurements of $\mathbf{E} \times \mathbf{B}$ drift together with EIA and ESF in the western American sector, *Whalen* [2001] suggested that when four coinciding thresholds are exceeded, the bubbles will be observed during equinox months at solar maximum. Later *Whalen* [2003] extended the previous equinox study to the entire year and showed that the equatorial anomaly is approximately linear with $\mathbf{E} \times \mathbf{B}$ drift, and ESF occurrence is dependent on and increases with maximum $\mathbf{E} \times \mathbf{B}$ drift velocity during the Equinox and June solstice period. Using simultaneous recordings of VHF scintillations, Faraday rotation, ionosonde measurements and magnetic field data in the Indian zone, *Dabas et al.* [2003] found that after the initial development of a plasma bubble, the $\mathbf{E} \times \mathbf{B}$ drift and the postsunset secondary maximum in inospheric electron density play an important role in the subsequent growth and evolution. Also, they suggested that the equatorial electrojet (EEJ) is a useful parameter for predicting the PBs development.

[6] When considering the association between the global-scale variations of EIA, PBs and prereversal $\mathbf{E} \times \mathbf{B}$ drift, earlier ground-based observations are of limited use because of the limited longitudinal coverage of land-masses around the magnetic equator. Space-based observations of the EIA, PBs and $\mathbf{E} \times \mathbf{B}$ drift have offered the ability to study the morphology on a global-scale. By using large databases from satellites such as AE-E, DMSP, KOMPSAT, ROCSAT, a large number of observational studies on EPBs and $\mathbf{E} \times \mathbf{B}$ drifts have been performed [e.g., *Kil and Heelis*, 1998; *McClure et al.*, 1998; *Huang et al.*, 2001; *Burke et al.*, 2004]. The longitudinal variations of PB occurrence show that the EPB occurrence is inhibited in the Pacific region during the December solstice and in the American-Atlantic region during the June solstice, and the seasonal variation is significant in the Pacific region [e.g., *Gentile et al.*, 2006; *Su et al.*, 2006]. By using DMSP, KOMPSAT density measurements, and plasma vertical drift model [*Scherliess and Fejer*, 1999], *Park et al.* [2005] investigated the effects of vertical drift on EPB occurrence. They found that the observed seasonal/longitudinal variations in EPB occurrence correlate with the modeled upward plasma drift. *Henderson et al.* [2005], using the GUVI observations, found that the crest-to-trough ratio (CTR) is well-correlated with EPB occurrence rate except in the Pacific sector during June solstice, where the occurrence rate is high and the CTR is low. Here we utilize the prereversal $\mathbf{E} \times \mathbf{B}$ drift and the plasma density obtained from ROCSAT-1, density measurements from DMSP and CHAMP satellites to investigate the seasonal/longitudinal distribution of PB occurrence rates, evening EIA and prereversal $\mathbf{E} \times \mathbf{B}$ drifts. This study shows that the small-scale longitudinal variations of low-latitude PB occurrence rates are better associated with the small-scale longitudinal structures of evening EIA and daytime EEJ. The main objective of this work is to examine the longitudinal correlation of evening EIA and prereversal $\mathbf{E} \times \mathbf{B}$ drifts for given seasons, and the dependence of PB occurrence on prereversal $\mathbf{E} \times \mathbf{B}$ drifts and evening EIA from simultaneous observations on magnetically quiet days (defined by an average $Kp < 3$).

2. Observations and Data Processing

[7] ROCSAT-1 was launched into a circular orbit at an altitude of ~600 km and carried instruments including the Ionospheric Plasma and Electrodynamics Instrument (IPEI), which is designed to take in situ measurements of ion density, temperature, composition, and drift velocity over a large dynamic range with high accuracy [*Yeh et al.*, 1999]. DMSP satellites are three-axis stabilized spacecraft that fly in Sun-synchronous, circular 98.7° inclination orbits at an altitude of ~840 km. The geographic local times of the orbits are either near

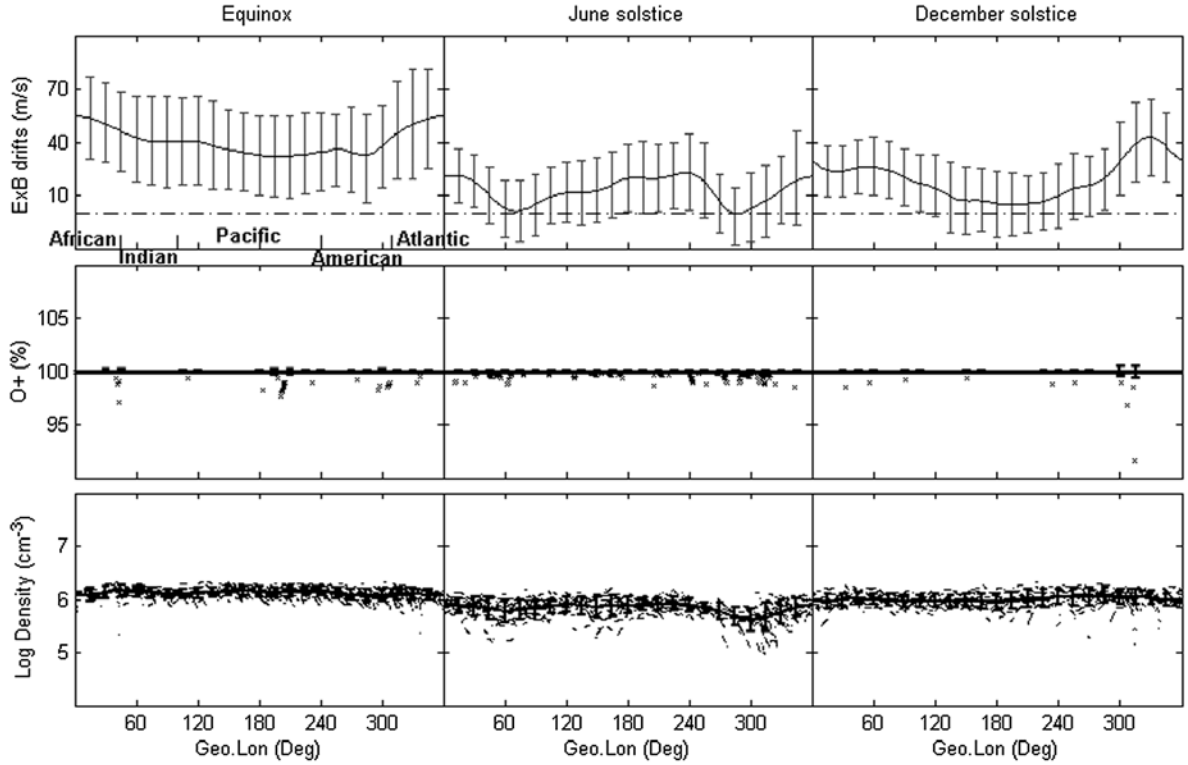

Figure 1. (Top) Seasonal and longitudinal variations of evening equatorial prereversal **E** × **B** drifts, (middle) percentage of the oxygen ions, and (bottom) the plasma density obtained from ROCSAT-1 for quiet conditions during solar maximum years (2000–2002). The vertical bars are the standard deviations.

18 h–06 h or 21 h–09 h local time meridians. Each satellite carries a suite of sensors called the Special Sensors-Ions, Electrons, and Scintillation (SSIES) to measure the densities, temperatures, and drifts of ionospheric ions and electrons [*Rich and Hairston*, 1994]. Here the density measurements from ROCSAT-1 (18 h–24 h LT) and DMSP-F15 (near 21 h LT) within magnetic latitude $|\mathrm{MLat}| < 20^\circ$ are used to study the plasma density irregularity structures.

[8] Although different criteria for identifying EPBs have been used in different studies [e.g., *Kil and Heelis*, 1998; *McClure et al.*, 1998; *Huang et al.*, 2001; *Su et al.*, 2006], the reported statistical results are similar. In order to perform comparisons between PB occurrence rates and **E** × **B** drift velocities, we used the criteria described in detail by *Su et al.* [2006]. Briefly, through an auto-search program, the ROCSAT 1 s (DMSP 4s) averaged ion density data is linearly detrended a 10 s (20 s) data segment, and a standard deviation value σ is obtained. The σ value reflects the roughness of a density structure and has a threshold value of 0.3% for identifying a plasma bubble.

[9] The electron density, obtained from a planar Langmuir probe mounted on the lower front panel of the CHAMP satellite [*McNamara et al.*, 2007], is used to characterize the individual EIA profiles. *Lühr et al.* [2007], using CHAMP density data, defined a crest-to-trough ratio (CTR) to characterize the EIA profile by a single number, $\mathrm{CTR} = (n_{cn} + n_{cs})/2n_t$, where n_{cn} and n_{cs} are the peak electron densities at the north and south crests, and n_t is the density at the equatorial trough. This ratio is suggested equivalent to the index used in total electron content studies [*Mendillo et al.*, 2000] and can be regarded as a measure of the strength of the equatorial fountain.

3. Results and Discussion

[10] To examine the global-scale dependence of evening EIA strength and PB occurrence rates on prereversal enhancements, we present the prereversal **E** × **B** drift velocity obtained from ion drift measurements from ROCSAT-1 (within 5 degrees of the magnetic equator). As *Kil et al.* [2007] reported, the accuracy of the velocity measurements from the ion drift meter on board the

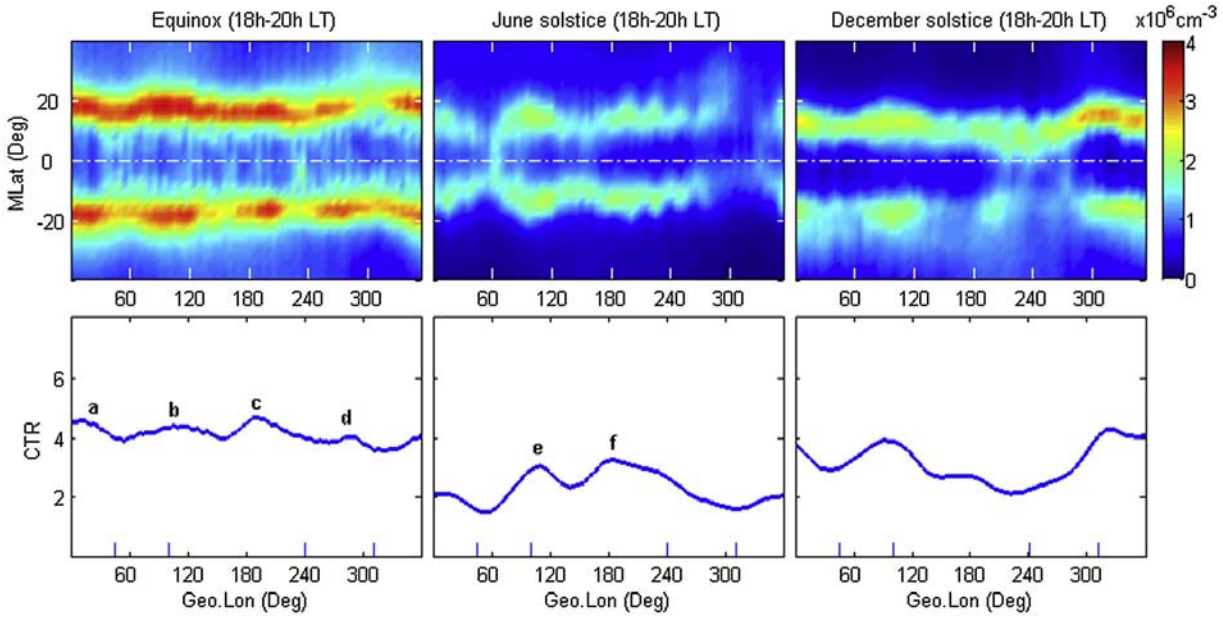

Figure 2. Season/Longitude-dependent structures of evening EIA (18–20 h LT). (Top) Distribution of the electron density from CHAMP for quiet conditions at solar maximum. (Bottom) The CTR index derived from the electron density profile (smooth curve of each panel is fitted to the 15° longitudinal mean values) shown above.

ROCSAT-1 depends on the total ion density and the proportion of oxygen ions. The cross-track ion velocity can be determined accurately (error < 10%) when the ion density is greater than 10^3 cm^{-3} and the percentage of the oxygen ion is greater than 85%. In the following study, the ion density, the percentage of the oxygen ion (O^+), and the averaged evening prereversal **E** × **B** drift velocity are obtained within the period 18 h–19 h LT.

[11] In Figure 1, the 15° longitudinal mean values of evening prereversal **E** × **B** drift velocity during Equinox (months 3–4, 9–10), June solstice (months 5–8) and December solstice (months 1–2, 11–12) are shown in the top panels. The vertical bars are the standard deviations. The percentage of O^+ and the plasma density are presented in the middle and bottom panels respectively. From these panels, it is seen that in most cases at 600 km, the condition (ion density and percentage of O^+ greater than 10^3 cm^{-3} and 85% respectively) is satisfied. The prereversal **E** × **B** drift pattern shows the seasonal/longitudinal variations are similar to the modeled equatorial vertical drift velocity (cf. Figure 9c of *Scherliess and Fejer* [1999]).

3.1. Association Between the Evening EIA and Prereversal E × B Drifts

[12] We now perform a direct comparison between the seasonal/longitudinal variations of the evening EIA and the prereversal **E** × **B** drifts. As shown in Figure 2, the CHAMP electron density data within period 18 h–20 h LT are sorted into longitude and latitude bins (top panels), the electron density peaks are located north and south of the magnetic equator, and the density trough is in between them. The 15° longitudinal mean values of EIA strength characterized by the CTR index are presented in the bottom panels.

[13] In general it can be clearly seen from Figures 1 and 2 that the evening EIA strength in the seasonal/longitudinal distribution is similar to the prereversal **E** × **B** drifts. During equinox, the evening prereversal **E** × **B** drifts, with a minimum average velocity of 30 m/s, are larger than the solstice drifts. Large-scale longitudinal changes of **E** × **B** drifts are evident during solstice. The June solstice **E** × **B** drifts have two apparent peaks centered in the Pacific (220°E), Atlantic and Africa (0°E) longitude regions respectively. For the December solstice, the maximum **E** × **B** drifts are shifted to Indian (60°E), American and Atlantic (300°E) regions. Correspondingly, the large-scale longitudinal variation of the evening EIA strength is evident during solstices, with peak values located in the Pacific, Atlantic and Africa regions (for June solstice), and the Indian, American and Atlantic sectors (for December solstice). As a whole, the evening EIA is strongest during equinox (the longitudinal averaged CTR index is larger than 4), intermediate during December solstice and weakest during June solstice. Similar results were reported by *Valladares*

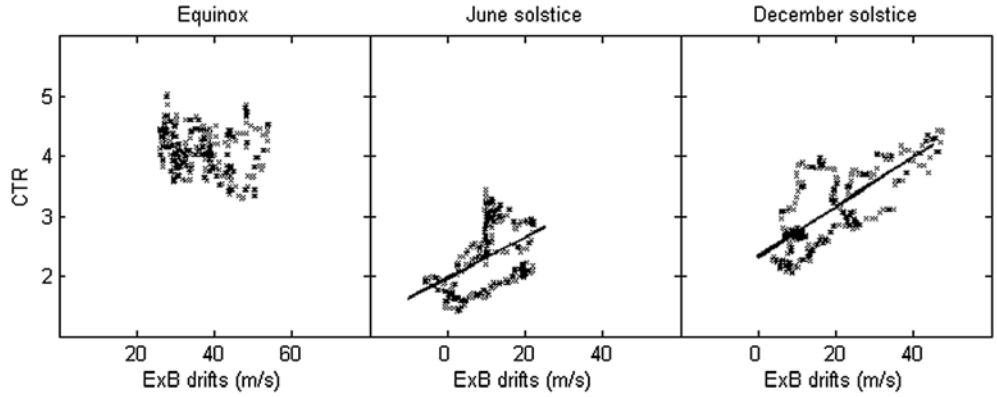

Figure 3. Plot of the evening EIA strength (CTR) and the prereversal **E** × **B** drift velocity for the same longitude.

et al. [2001]. By using a chain of GPS receivers located in the Western American sector, they found that the anomaly was greatest in latitude and TEC level near the equinoxes, least near June solstice, and intermediate near December solstice.

[14] Figure 3 shows the evening EIA strength (CTR) associated with the evening prereversal **E** × **B** drift velocity for the same longitude grid. A clear relation exists between the magnitude of the prereversal enhancement and the EIA strength: larger prereversal enhancement presents, the EIA are much stronger. In the equinoctial months, the drift velocity and the EIA strength are greater than 30 m/s and 4 respectively. During solstices, the EIA strength increases with the increasing drift velocity. As a whole, it probably indicates that the EIA strength is linear in **E** × **B** drift velocity, and shows consistency in the observed [*Whalen*, 2003, 2004] and modeled [*Basu et al.*, 2004] results. By analyzing the Nemax (maximum F layer electron density) measured by eight ionospheric sounders, which were located in the

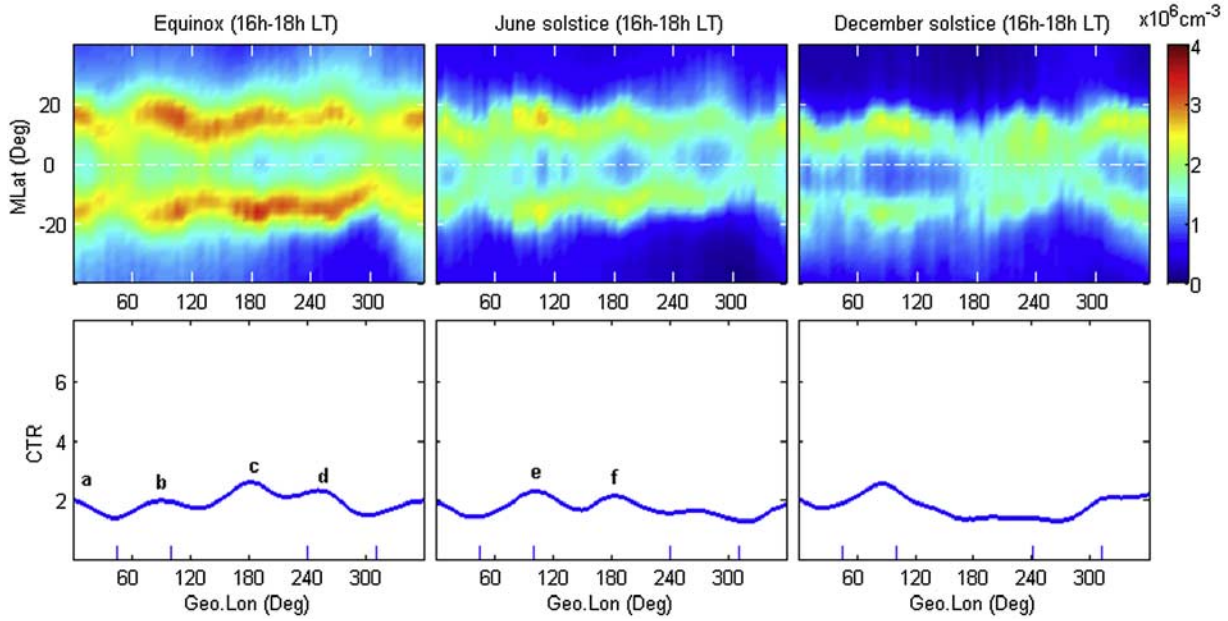

Figure 4. Same as Figure 2 but for afternoon EIA (16–18 h LT). Figures 2 and 4 show that the seasonal distribution in the evening EIA is apparently stronger than that in the afternoon EIA for nearly all longitudes, but the wave-like small-scale variation in longitudinal distribution between them is similar, especially during equinox.

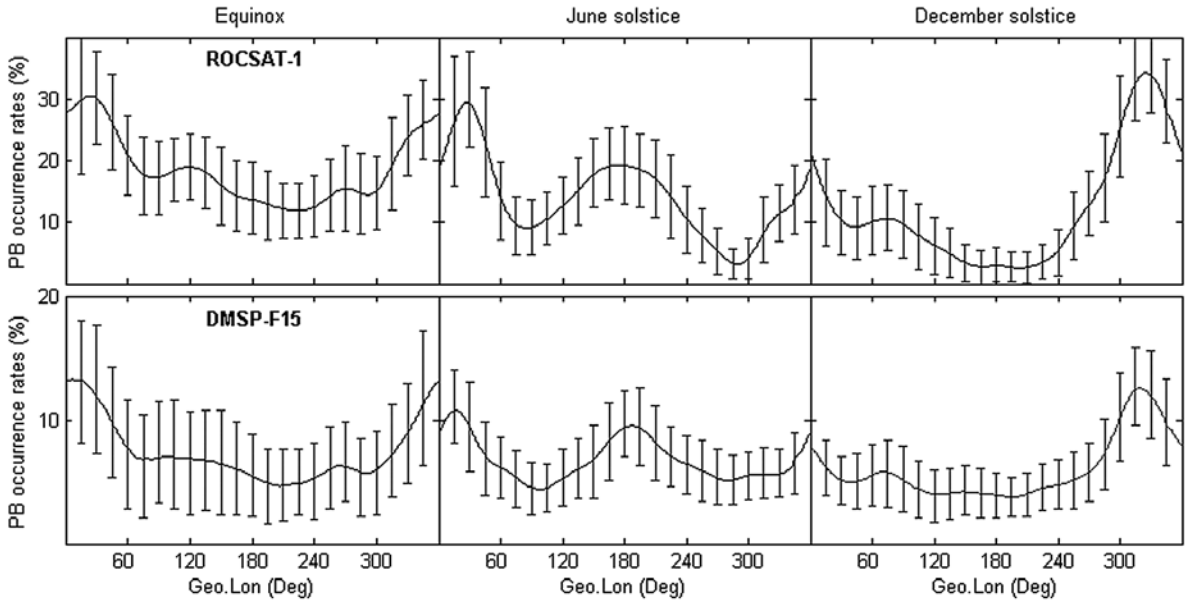

Figure 5. Seasonal and longitudinal variation of equatorial plasma bubble (EPB) occurrence (|MLat| < 10°). (Top) EPB occurrence obtained from ROCSAT-1 for quiet conditions at solar maximum. (Bottom) Same as top panels but obtained from DMSP-F15. The large-scale variations in longitudinal distribution of EPB occurrence rates are similar to the prereversal **E** × **B** drifts.

anomaly regions in eastern Asia, the Pacific, and South America, *Whalen* [2004] found that Nemax is linear with **E** × **B** drift speed at each station with functional dependence that varies with latitude and longitude. On the basis of the low-latitude density model of Air Force Research Laboratory (AFRL) and the drift measurements from Jicamarca incoherent scatter radar, *Basu et al.* [2004] reported that there exists a linear relationship between the maximum postsunset plasma drift velocity and the peak-to-valley ratio of anomaly TEC, and they suggested that the linear relationship may be used to estimate the maximum postsunset velocity from the peak-to-valley ratios of anomaly TEC.

[15] When we note the small-scale longitude structures of evening EIA, such as the wave number-4 structure during Equinox, it is found that the structure exists before the occurrence of the prereversal enhancement. As shown in Figures 2 and 4, the small-scale longitude variation of evening (18 h–20 h LT) EIA strength is similar to the afternoon (16 h–18 h LT) EIA strength during equinox, and are marked as a, b, c, d, e and f in these two figures. By using late afternoon TOPEX TEC measurements, *Vladimer et al.* [1999] showed that the TEC in the EIA region displays longitudinal variability which extends over 4 hours of LT and is repeated day-to-day during magnetically quiet conditions. Here the similarities between four peaked longitude structures of evening EIA and afternoon EIA, probably indicate that the observed small-scale longitudinal variations of evening EIA are associated with the daytime EIA small-scale longitude structures. On the basis of the measurements from IMAGE and TIMED satellites, *Sagawa et al.* [2005] and *England et al.* [2006a] examined the global characteristics of postsunset EIA, and found four peaked wave-like longitudinal variation during Equinox. Through an analysis of two data sets and GWSM-02 model, *England et al.* [2006b] reported that the four peaked longitudinal variation of postsunset EIA is created by a process occurring in the dayside ionosphere, and the predicted modulation of the dayside thermospheric winds and temperatures at *E* region altitudes (created by nonmigrating diurnal tides) can explain the modulation in the dayside equatorial fountain.

[16] Comparison of Figures 2 and 4 show that the seasonal distribution of the evening EIA is stronger than afternoon EIA strength for nearly all longitudes. The good agreement between the large-scale longitudinal variation of evening EIA and prereversal **E** × **B** drifts, and the enhanced EIA strength around sunset indicate a positive correlation between the prereversal enhancement and EIA. The prereversal **E** × **B** drifts enhance the equatorial fountain and increase the plasma density at off-equatorial latitudes, thus give rise to large ionization anomaly during postsunset hours, as indicated by the larger CTR index presented in Figure 2 as compared to Figure 4. Some small-scale variations in longitudinal

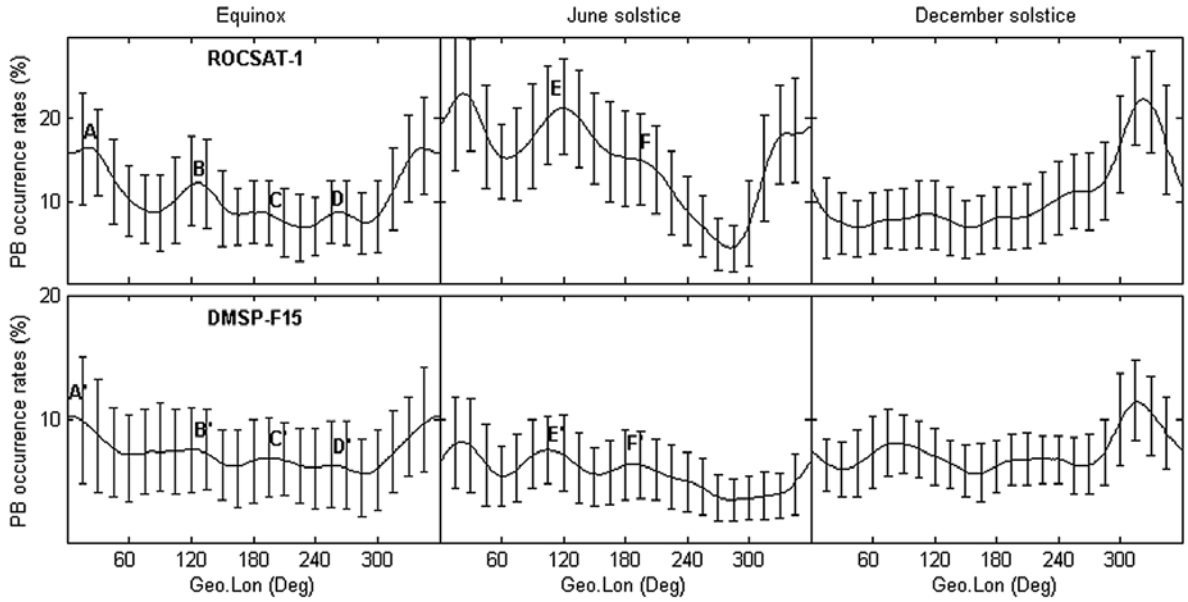

Figure 6. Same as Figure 5 but for low-latitude plasma bubble (LPB) occurrence ($10° \leq |\text{MLat}| < 20°$). The small-scale variations in longitudinal distribution of LPB occurrence rates (labeled A, B, C, D, E, and F and A′, B′, C′, D′, E′, and F′) are similar to the evening EIA.

distribution of evening EIA, are found to be consistent with the longitudinal variations of afternoon EIA.

3.2. Dependence of PB Occurrence Rates on Prereversal E × B Drifts and EIA

[17] In this section, we shall describe the characteristics of the observed plasma bubbles (PBs), and analyze the dependence of PB occurrence on prereversal $\mathbf{E} \times \mathbf{B}$ drifts and evening EIA in three sets of observations. Taking into consideration the global structures, the seasonal/longitudinal statistical occurrence distribution of density irregularities have been studied by many authors [e.g., *Kil and Heelis*, 1998; *McClure et al.*, 1998; *Huang et al.*, 2001; *Burke et al.*, 2004; *Gentile et al.*, 2006; *Su et al.*, 2006]. Here we focus on the correlative study between them. First we simply depict the large-scale seasonal/longitudinal variation of PB occurrence rates. As shown in Figures 5 and 6, the PB occurrence rates within the equatorial and low-latitude regions for ROCSAT-1 and DMSP F15 measurements are recorded. The smooth curve of each panel is fitted to the 15° longitudinal mean values, and the vertical bars are the standard deviations. In general the features of the seasonal/longitudinal variations of PB occurrence rates obtained from ROCSAT-1 and DMSP F15 are similar.

[18] Figures 5 and 6, together with Figure 1, indicate that the equatorial and low-latitude PB percentage occurrence rate shows correspondence with the large-scale longitudinal distribution of prereversal $\mathbf{E} \times \mathbf{B}$ drift velocity. Previous studies have shown that the bubble occurrence rate increases with the increasing prereversal $\mathbf{E} \times \mathbf{B}$ drift. Using KOMPSAT-1 and DMSP F15 density measurements, and the vertical drift estimated from the drift model [*Scherliess and Fejer*, 1999], *Park et al.* [2005] examined the relationship of EPBs distribution and the vertical plasma drift, and reported that the longitudinal variation of EPBs is well-correlated with the upward drift during equinox and June solstice. On the basis of the ion density and drift measurements from ROCSAT-1, DMSP F13 and F15, *Li et al.* [2007] investigated the large-scale seasonal/longitudinal dependence and the latitudinal extent of PB occurrence on prereversal enhancement. A clear linear correlation exists between the magnitude of the prereversal enhancement and the equatorial and low-latitude PB occurrence rate. The results indicate that the larger prereversal $\mathbf{E} \times \mathbf{B}$ drifts, by lifting the F layer to higher altitudes where the recombination effects are negligible and collisions are rare, result in a condition conducive to the development of plasma irregularities. Also, through the Generalized Rayleigh-Taylor (GRT) instability mechanism, the depleted plasma bubbles rise to higher altitudes and extend to higher latitudes along the magnetic field lines.

[19] On the other hand, taking into account the small-scale longitudinal variations, it can be seen that the small-scale wave-like variations in longitude dis-

tribution of low-latitude plasma bubble (LPB, $10^\circ \leq |\text{MLat}| < 20^\circ$) occurrence rate is obvious, and marked as A, B, C, D, E and F for ROCSAT-1, and A′, B′, C′, D′, E′ and F′ for DMSP F15. These wave-like variations in longitudinal distribution of LPB occurrence rates are similar to the evening EIA for given seasons. Using the GUVI observations during years 2002–2003, *Henderson et al.* [2005] found that the EPB occurrence rate in longitudinal distribution is well-correlated with CTR for a given season and year, but the Pacific sector is unique in that the CTR is low yet EPB occurrence rate is high during June solstice. This phenomenon can be seen from Figures 2 and 5. As shown in the top and bottom of Figure 2, lower CTR values are observed in the Pacific regions during June solstice (located between e and f labeled regions), and the high EPB occurrence rate in the whole Pacific sector is shown in Figure 5, which is consistent with the high prereversal **E** × **B** drifts in that sector. A possible explanation could be that the **E** × **B** drifts enhance the RT instability and play the main role for the development of PBs.

[20] Together with earlier studies and observational results presented in Figures 1, 5 and 6, it is seen that the PB occurrence rates and prereversal **E** × **B** drifts show the similar large-scale variation in longitudinal distribution for a given season. For the small-scale structure seen in the longitudinal distribution of LPB occurrence rates, it exhibits a good agreement with the evening EIA. These observational results indicate that the large-scale longitudinal variation of PB occurrence rates result from the prereversal **E** × **B** drift, and the small-scale longitudinal variation is probably induced by the small-scale longitudinal structure of evening EIA.

3.3. Discussion

[21] In previous sections we have seen that the large-scale variations in seasonal/longitudinal distribution of evening EIA strength and PB occurrence rates are similar to evening prereversal **E** × **B** drifts, because of the same main driving source of prereversal *F* region electric field enhancement over the magnetic equator. The prereversal electric field enhancement is produced by the interaction of the evening eastward thermospheric wind with the longitudinal E layer Pedersen conductivity that exists across the sunset terminator [*Abdu*, 1997]. The rapid evening enhancement in the zonal electric field leads to large vertical drifts, thereby lifting the F layer to altitudes where the condition is conducive to the development of plasma irregularities. Also, the large evening vertical drifts cause the resurgence of the equatorial fountain, and increase the plasma density at off-equatorial latitudes.

[22] Despite the similarities between large-scale variation in longitudinal distribution of PB occurrence rates, evening EIA strength and prereversal **E** × **B** drifts for a given season, the discrepancies exist in small-scale longitudinal variations. Using simultaneous recordings of VHF scintillations at five locations situated in Indian sector, *Dabas et al.* [2003] examined the scintillation occurrence, **E** × **B** drift speed and EEJ, and found that the scintillation shows positive correlation with daytime (1100 LT) EEJ strength. Here we shall adopt the EEJ strength modeled by *Alken and Maus* [2007], which were derived from CHAMP observations, to investigate the dependence of small-scale wave-like variation in longitudinal distribution of PB occurrence rates on evening EIA and daytime EEJ. The results are shown in Figure 7.

[23] The prereversal **E** × **B** drifts, EIA strength and PB occurrence rates presented in Figure 7 are the mean values derived from Figures 1, 2, 5, and 6. From Figure 7, it is seen that during equinox, the peaked longitude structure in the LPB occurrence rates (labeled A, B, C and D) and CTR index (labeled a, b, c and d) are in good agreement with daytime EEJ (labeled a′, b′, c′ and d′). During the solstices, correspondence between LPB occurrence rates (labeled E and F) and EIA strength (labeled e and f) was also observed, and correspond well with daytime EEJ peaks (e′ and f′). Results of the figure indicate that the wave-like longitudinal variation of EEJ may be responsible for the small-scale variations in longitudinal distribution of LPB occurrence rates, especially during equinox. By comparing the postsunset EIA obtained from IMAGE and TIMED satellites with EEJ obtained from CHAMP, Ørsted and SAC-C measurements, *England et al.* [2006a] found the postsunset EIA and daytime EEJ show similar wave-like longitudinal variation during equinox, and a strong vertical coupling between the ionosphere and troposphere was suggested. Using simultaneous observations of the electron density and zonal wind obtained from CHAMP satellite, *Lühr et al.* [2007] found that the EIA and the zonal delta wind show a persistent and dominant 4-peaked longitudinal variation. Considering the zonal winds are the prime driver of the *F* region dynamo, they suggested that the wave-4 pattern should be visible in all phenomena influenced by the *F* region dynamo. According to the GRT equation [*Sultan*, 1996], the growth rate of the instability is proportional to the product $(\nabla N/N) \times N$ integrated through the ionosphere [e.g., *Aarons et al.*, 1981; *Rino and Liu*, 1982; *Wernik et al.*, 1983]. A strong EIA gives rise to large ionization anomaly gradients ($\nabla N/N$) in the postsunset time frame, which enhances PB development associated with intense scintillation. Hence for the observed small-scale longitudinal variation of LPBs, it is probably induced by the small-scale variation in longitudinal distribution of EIA, which is determined by the coupling process between ionosphere and troposphere as *England et al.* [2006a, 2006b] suggested. The source of the small-scale signature in EIA and EEJ is the modulation

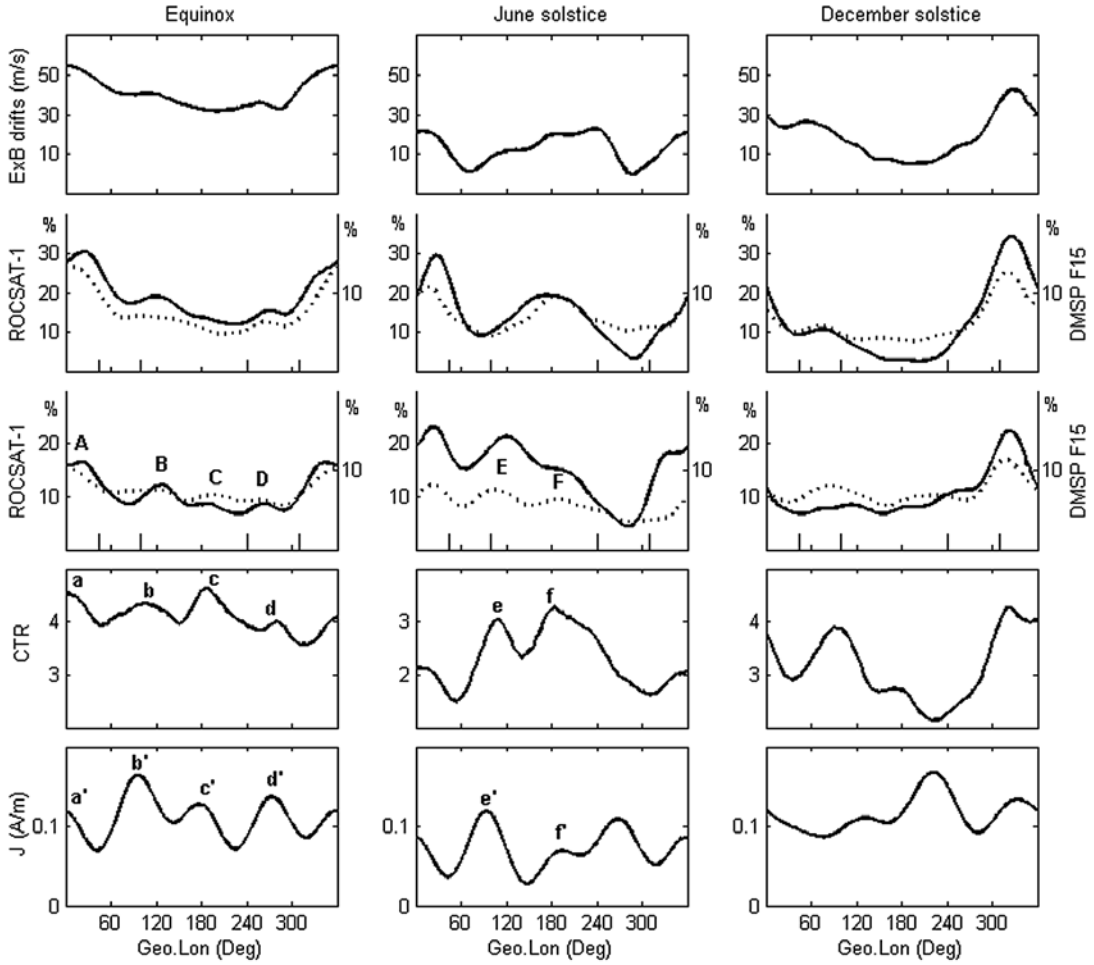

Figure 7. Plot of the (first row) prereversal **E** × **B** drifts, (second row) EPB occurrence rates, (third row) LPB occurrence rates, and (fourth row) evening EIA strength index derived from Figures 1, 5, 6, and 2 and (fifth row) EEJ strength from the empirical EEJ model.

of the daytime *E* region dynamo fields and the associated vertical drifts in the *F* region ionosphere.

4. Summary

[24] From all of above results and discussion, this paper reports the association of large-scale variations of evening EIA, PB occurrence rates in longitudinal distribution with evening prereversal **E** × **B** drifts, and the dependence of small-scale longitudinal variations of LPB occurrence rates on evening EIA and daytime EEJ for given seasons. The main conclusions are summarized as follows, (1) The good agreement between the large-scale variations in seasonal/longitudinal distribution of PB occurrence rates, evening EIA and prereversal **E** × **B** drifts, indicates that the prereversal **E** × **B** drifts provide the most likely mechanism responsible for the global large-scale variations in longitudinal distribution of evening EIA enhancement and PB occurrence rates. (2) Both ROCSAT-1 and DMSP F15 instruments observed small-scale wave-like variation in longitudinal distribution of LPB occurrence rates. The locations of these small-scale wave-like peaks are similar to those of the strong evening EIA. It probably indicates that the wave-like variation in longitudinal distribution of LPB occurrence is controlled by the small-scale variation of evening EIA. The small-scale structures of evening EIA give rise to small-scale variations in longitudinal distribution of ionization anomaly gradients ($\nabla N/N$) in the postsunset region, and then affect the longitudinal distribution of PB

development through the RT instability. The small-scale structure of the evening EIA was suggested to be linked with the variation of daytime EEJ [*England et al.*, 2006a]. (3) On the basis of the similarity of longitudinal dependence, the large-scale longitudinal variation of PB occurrence rate and the evening EIA seem to be a function of evening prereversal **E** × **B** drift velocity, and the small-scale longitudinal variation of LPB occurrence rates is dependent on the longitudinal distribution of evening EIA. Further study on the role of evening prereversal **E** × **B** drifts, evening EIA and daytime EEJ on the occurrence of PBs is helpful for understanding the distribution of equatorial and low-latitude ionospheric scintillation.

[25] **Acknowledgments.** Special thanks to Dr. J. Lei of the High Altitude Observatory, National Center for Atmospheric Research, USA, for his valuable suggestions and helpful discussions. This work was supported by National Natural Science Foundation of China (40774091, 40574072, and 40725014) and the KIP Pilot Project (KZCX3-SW-144) of Chinese Academy of Sciences. The authors acknowledge SPIDR for providing the Kp index and thank D. Cooke and Ch. Roth for processing the CHAMP PLP data. The CHAMP mission is supported by the German Aerospace Center in operation and by the Federal Ministry of Education and Research in data processing.

References

Aarons, J., H. E. Whitney, E. MacKenzie, and S. Basu (1981), Microwave equatorial scintillation intensity during solar maximum, *Radio Sci.*, *16*, 939–945.

Abdu, M. A. (1997), Major phenomena of the equatorial ionosphere-thermosphere system under disturbed conditions, *J. Atmos. Sol.-Terr. Phys.*, *59*, 1505–1519.

Alex, S., P. V. Koparkar, and R. G. Rastogi (1989), Association between equatorial and tropical spread-F, *J. Atmos. Terr. Phys.*, *51*, 371–379.

Alex, S., H. Chandra, and R. G. Rastogi (2003), Association between equatorial and tropical spread-F, *Indian J. Radio Space Phys.*, *32*, 83–92.

Alken, P., and S. Maus (2007), Spatio-temporal characterization of the equatorial electrojet from CHAMP, Ørsted, and SAC-C satellite magnetic measurements, *J. Geophys. Res.*, *112*, A09305, doi:10.1029/2007JA012524.

Anderson, D. N., B. Reinisch, C. E. Valladares, J. Chau, and O. Veliz (2004), Forecasting the occurrence of ionospheric scintillation activity in the equatorial ionosphere on day-to-day basis, *J. Atmos. Sol.-Terr. Phys.*, *66*, 1567–1572.

Basu, S., et al. (1996), Scintillations, plasma drifts, and neutral winds in the equatorial ionosphere after sunset, *J. Geophys. Res.*, *101*, 26,795–26,809.

Basu, B., J. M. Retterer, O. de La Beaujardière, C. E. Valladares, and E. Kudeki (2004), Theoretical relationship between maximum value of the post-sunset drift velocity and peak-to-valley ratio of anomaly TEC, *Geophys. Res. Lett.*, *31*, L03807, doi:10.1029/2003GL018725.

Burke, W. J., L. C. Gentile, C. Y. Huang, C. E. Valladares, and S.-Y. Su (2004), Longitudinal variability of equatorial plasma bubbles observed by DMSP and ROCSAT, *J. Geophys. Res.*, *109*, A12301, doi:10.1029/2004JA010583.

Dabas, R. S., L. Singh, D. R. Lakshmi, P. Subramanyam, P. Chopra, and S. C. Garg (2003), Evolution and dynamics of equatorial plasma bubbles: Relationships to E × B drift, postsunset total electron content enhancements, and equatorial electrojet strength, *Radio Sci.*, *38*(4), 1075, doi:10.1029/2001RS002586.

Dabas, R. S., L. Singh, S. C. Garg, R. M. Das, K. Sharma, and V. K. Vohra (2006), Growth and decay of a post-sunset equatorial anomaly at low latitudes: Control of E × B, neutral winds and daytime electrojet strength, *J. Atmos. Terr. Phys.*, *68*, 1622–1632.

England, S. L., S. Maus, T. J. Immel, and S. B. Mende (2006a), Longitudinal variation of the *E*-region electric fields caused by atmospheric tides, *Geophys. Res. Lett.*, *33*, L21105, doi:10.1029/2006GL027465.

England, S. L., T. J. Immel, E. Sagawa, S. B. Henderson, M. E. Hagan, S. B. Mende, H. U. Frey, C. M. Swenson, and L. J. Paxton (2006b), Effect of atmospheric tides on the morphology of the quiet time, postsunset equatorial ionospheric anomaly, *J. Geophys. Res.*, *111*, A10S19, doi:10.1029/2006JA011795.

Fejer, B. G., L. Scherliess, and E. R. de Paula (1999), Effects of the vertical plasma drift velocity on the generation and evolution of equatorial spread F, *J. Geophys. Res.*, *104*, 19,859–19,869.

Garg, S. C., Y. V. Somayajulu, L. Singh, and T. R. Tyagi (1983), Evidence of the development and decay of a post-sunset equatorial anomaly at low latitudes, in *Proceedings of International Symposium on Beacon Satellite Studies of the Earth Environment*, edited by T. R. Tyagi, pp. 359–373, Natl. Phys. Lab., New Delhi, India.

Gentile, L. C., W. J. Burke, and F. J. Rich (2006), A climatology of equatorial plasma bubbles from DMSP 1989–2004, *Radio Sci.*, *41*, RS5S21, doi:10.1029/2005RS003340.

Gupta, J. K., L. Singh, and R. S. Dabas (2002), Faraday polarization fluctuations and their dependence on post sunset secondary maximum and amplitude scintillations at Delhi, *Ann. Geophys.*, *20*, 185–190.

Henderson, S. B., C. M. Swenson, A. B. Christensen, and L. J. Paxton (2005), Morphology of the equatorial anomaly and equatorial plasma bubbles using image subspace analysis of Global Ultraviolet Imager data, *J. Geophys. Res.*, *110*, A11306, doi:10.1029/2005JA011080.

Huang, C. Y., W. J. Burke, J. S. Machuzak, L. C. Gentile, and P. J. Sultan (2001), DMSP observations of equatorial plasma bubbles in the topside ionosphere near solar maximum, *J. Geophys. Res.*, *106*, 8131–8142.

Kelley, M. C. (1989), *The Earth's Ionosphere, Plasma Physics and Electrodynamics*, Academic, San Diego, Calif.

Kil, H., and R. A. Heelis (1998), Global distribution of density irregularities in the equatorial ionosphere, *J. Geophys. Res.*, *103*, 407–420.

Kil, H., S.-J. Oh, M. C. Kelley, L. J. Paxton, S. L. England, E. Talaat, K.-W. Min, and S.-Y. Su (2007), Longitudinal structure of the vertical E × B drift and ion density seen from ROCSAT-1, *Geophys. Res. Lett.*, *34*, L14110, doi:10.1029/2007GL030018.

Li, G., B. Ning, L. Liu, Z. Ren, J. Lei, and S.-Y. Su (2007), The correlation of longitudinal/seasonal variations of evening equatorial pre-reversal drift and of plasma bubbles, *Ann. Geophys.*, *25*, 2571–2578.

Lühr, H., K. Haüsler, and C. Stolle (2007), Longitudinal variation of *F* region electron density and thermospheric zonal wind caused by atmospheric tides, *Geophys. Res. Lett.*, *34*, L16102, doi:10.1029/2007GL030639.

McClure, J. P., S. Singh, D. K. Bamgboye, F. S. Johnson, and H. Kil (1998), Occurrence of equatorial *F* region irregularities: Evidence for tropospheric seeding, *J. Geophys. Res.*, *103*, 29,119–29,129.

McNamara, L. F., D. L. Cooker, C. E. Valladares, and B. W. Reinisch (2007), Comparison of CHAMP and Digisonde plasma frequencies at Jicamarca, Peru, *Radio Sci.*, *42*, RS2005, doi:10.1029/2006RS003491.

Mendillo, M., L. Bosheng, and J. Aarons (2000), The application of GPS observations to equatorial aeronomy, *Radio Sci.*, *35*, 885–904.

Park, J., K. W. Min, V. P. Kim, H. Kil, J.-J. Lee, H.-J. Kim, E. Lee, and D. Y. Lee (2005), Global distribution of equatorial plasma bubbles in the premidnight sector during solar maximum as observed by KOMPSAT-1 and Defense Meteorological Satellite Program F15, *J. Geophys. Res.*, *110*, A07308, doi:10.1029/2004JA010817.

Rich, F. J., and M. Hairston (1994), Large-scale convection patterns observed by DMSP, *J. Geophys. Res.*, *99*, 3827–3844.

Rino, C., and C. Liu (1982), Intensity scintillation parameters for characterizing transionospheric radio signals, *Radio Sci.*, *17*, 279–284.

Sagawa, E., T. J. Immel, H. U. Frey, and S. B. Mende (2005), Longitudinal structure of the equatorial anomaly in the nighttime ionosphere observed by IMAGE/FUV, *J. Geophys. Res.*, *110*, A11302, doi:10.1029/2004JA010848.

Scherliess, L., and B. G. Fejer (1999), Radar and satellite global equatorial *F* region vertical drift model, *J. Geophys. Res.*, *104*, 6829–6842.

Su, S.-Y., C. H. Lin, H. H. Ho, and C. K. Chao (2006), Distribution characteristics of topside ionospheric density irregularities: Equatorial versus midlatitude regions, *J. Geophys. Res.*, *111*, A06305, doi:10.1029/2005JA011330.

Sultan, P. J. (1996), Linear theory and modeling of the Rayleigh-Taylor instability leading to the occurrence of equatorial spread *F*, *J. Geophys. Res.*, *101*(A12), 26,875–26,891.

Tulasi Ram, S., P. V. S. Rama Rao, K. Niranjan, D. S. V. V. D. Prasad, R. Sridharan, C. V. Devasia, and S. Ravindran (2006), The role of post-sunset vertical drifts at the equator in predicting the onset of VHF scintillations during high and low sunspot activity years, *Ann. Geophys.*, *24*, 1609–1616.

Valladares, C. E., S. Basu, K. Groves, M. P. Hagan, D. Hysell, A. J. Mazella, and R. E. Sheehan (2001), Measurement of the latitudinal distributions of total electron content during equatorial spread F events, *J. Geophys. Res.*, *106*, 29,133–29,152.

Vladimer, J. A., P. Jastrzebski, M. C. Lee, P. H. Doherty, D. T. Decker, and D. N. Anderson (1999), Longitudinal structure of ionospheric total electron content at low latitudes measured by the TOPEX/Poseidon satellite, *Radio Sci.*, *34*, 1239–1260.

Walker, G. O. (1981), Longitudinal structure of the *F* region equatorial anomaly: A review, *J. Atmos. Terr. Phys.*, *43*, 763–774.

Wernik, A. W., C. H. Liu, and K. C. Yeh (1983), Modeling of spaced-receiver scintillation measurements, *Radio Sci.*, *18*, 743–764.

Whalen, J. A. (2000), An equatorial bubble: Its evolution observed in relation to bottomside spread F and to the Appleton anomaly, *J. Geophys. Res.*, *105*, 5303–5315.

Whalen, J. A. (2001), The equatorial anomaly: Its quantitative relation to equatorial bubbles, bottomside spread F and E × B drift velocity during a month at solar maximum, *J. Geophys. Res.*, *106*, 29,125–29,132.

Whalen, J. A. (2003), Dependence of the equatorial anomaly and of equatorial spread F on the maximum prereversal E × B drift velocity measured at solar maximum, *J. Geophys. Res.*, *108*(A5), 1193, doi:10.1029/2002JA009755.

Whalen, J. A. (2004), Linear dependence of the postsunset equatorial anomaly electron density on solar flux and its relation to the maximum prereversal E × B drift velocity through its dependence on solar flux, *J. Geophys. Res.*, *109*, A07309, doi:10.1029/2004JA010528.

Woodman, R. F., and C. LaHoz (1976), Radar observations of *F* region equatorial irregularities, *J. Geophys. Res.*, *81*, 5447–5466.

Yeh, H. C., S. Y. Su, Y. C. Yeh, J. M. Wu, R. A. Heelis, and B. J. Holt (1999), Scientific mission of the IPEI payload onboard ROCSAT, *Terr. Atmos. Oceanic Sci.*, suppl., 19–42.

G. Li, L. Liu, B. Ning, X. Yue, and B. Zhao, Institute of Geology and Geophysics, Chinese Academy of Sciences, Beijing 100029, China. (gzlee@mail.iggcas.ac.cn; lliu@mail.iggcas.ac.cn; nbq@mail.iggcas.ac.cn; yuexinan@mail.iggcas.ac.cn; zbqjz@mail.iggcas.ac.cn)

S.-Y. Su, Institute of Space Science, National Central University, Chung-Li, Taiwan. (sysu@jupiter.ss.ncu.edu.tw)

S. Venkatraman, William B. Hanson Center for Space Sciences, University of Texas at Dallas, Richardson, TX, USA. (sarita@utdallas.edu)